**SASEC2015**
**Third Southern African Solar Energy Conference**
**11 – 13 May 2015**
**Kruger National Park, South Africa**

# P3HT:PCBM BASED SOLAR CELLS: A SHORT REVIEW FOCUSING ON ZNO NANOPARTICLES BUFFER LAYER, POST-FABRICATION ANNEALING AND AN INVERTED GEOMETRY

Mbule P.S.[1]*, H.C. Swart[2], O.M. Ntwaeaborwa[2]*, M.S. Dhlamini[1] and B.M. Mothudi[1]
[1]Department of Physics, University of South Africa, P.O. Box 392, 0003, South Africa ,
[2]Department of Physics, University of the Free State, P.O.Box339, Bloemfontein, 9300 South Africa
*E-mail: mbuleps@unisa.ac.za, ntwaeab@ufs.ac.za

## ABSTRACT

Today, bulk heterojunction (BHJ) organic solar cells (OSCs) dominate modern age research in renewable solar energy. In recent developments, the ultimate goal is to improve the general performance of the BHJ-OSCs to enable them to compete on an equal footing basis with conventional silicon photovoltaic cells. In this presentation, we review the fundamental parameters that have been reported to improve the general performance of the BHJ-OSC devices. These parameters include, among other things, the use ZnO nanoparticles electron transport layer (ETL) inserted between the top electrode and the photoactive layer, annealing procedure and device geometry.

The BHJ-OSC devices constructed in this study comprised of successive (bottom up) layers of (3,4ethylenedioxythiophene):poly(styrenesulfonate) (PEDOT:PSS), a blend of poly(3-hexylthiophene) (P3HT) and [6,6]-phenyl butyric acid methyl ester (PCBM) layer, zinc oxide (ZnO) nanoparticles and aluminum (Al) metal top electrode. These layers were deposited on indium tin oxide (ITO) coated glass substrates. The device construction was also inverted (top down) in order to evaluate the effect of inversion on the power conversion efficiency and the general performance of the devices. The devices were annealed at 155 oC either before (pre-annealed) or after (post-annealed) the deposition of the Al top electrode. Post-annealed devices showed improved photovoltaic (PV) characteristics when compared to pre-annealed devices. Furthermore, we discuss the performance of inverted geometry in comparison to ZnO nanoparticles and nanoflakes as buffer layers.

## INTRODUCTION

Organic solar cells (OSCs) based on nanostructured composites of electron donor and acceptor materials promise to deliver future solutions to the low-cost energy generation. Bulk-heterojunction devices based on polymer-fullerene blends already demonstrate power conversion efficiencies exceeding 5 % [1]. Although polymer-fullerene based devices exhibit excellent photovoltaic (PV) properties, their power conversion efficiency (PCE) is still low compared to that of the conventional silicon PV cells and this is the major limitation for their faster commercialization [2]. Normal/conventional geometry of BHJ-OSCs can suffer from degradation of photo-active layer due to penetration of oxygen and water molecules through the top electrode via pin holes or grain boundaries [3]. Again, the oxidation of the low work function layer in the cathode contact and/or photo-oxidation of the active materials degrade the performance of the photovoltaic cells by lowering the open-circuit voltage ($V_{oc}$), short-circuit current density ($J_{sc}$) and fill factor (FF). In addition, the Al atoms from the top electrode may diffuse into the active layer and act as quenching/recombination centers [3]. To overcome these limitations, the transparent and conductive interfacial layers, which are inserted between the photo-active layer (P3HT:PCBM) and top metal electrode (Al), are required. Inorganic semiconducting materials such as TiO2 or ZnO [4-5], are often used as electron transporting layer (ETL) or /and buffer layer. The role of this ETL is to facilitate electrons between the active layer and at the same time block holes from reaching the top metal electrode and they can also act to prevent diffusion of the top electrode metal ions into the photoactive layer. In addition, to also form an electrical contact to a less air sensitive high work function metal such as Ag or Au. ZnO is one of the mostly used functional materials with a wide and direct band gap (3.37 eV at room temperature), high exciton binding energy (60 meV) and thermal stability as opposed to $TiO_2$, making it the best candidate for applications particularly in solar cells [6]. It can be synthesized by a number of methods such as chemical bath deposition, laser ablation, hydrothermal process, co-precipitation and sol-gel at low production costs [7-11]. However, most of these synthesis techniques involve processes of many complex steps requiring sophisticated equipment and extremely thorough experimental conditions. Wet-chemistry colloid preparation as opposed to other methods, have its own attractiveness and ZnO nanostructures can be synthesized easily at low costs. Wet-chemistry route also allow the control of particle size, size

distribution, shape and structures under different experimental conditions [12].

The efficiency of polymer photovoltaic devices is mainly limited by the low carrier mobility and short exciton diffusion lengths of polymers. However, significant advances in PCE can be attained by understanding the fundamental electronic interaction between the polymeric donors and the fullerene acceptors as well as complex interplay of device architecture, morphology, processing and electronic processes. Recent advances such as thermal annealing of BHJ-OSCs can help improve the photo-active morphology and charge carrier mobility, thereby increasing the quantum efficiency of devices [13]. In addition the sequence of thermal treatment is critical for the device performance and result in some unique properties of P3HT over other polymers, including high degree of crystallinity at nanoscale, high hole mobility in regioregular state (10-4 to 10-2 $cm^2/Vs$), extended absorption in the red region (to 650 nm) and environmental stability [14]. Furthermore, thermal annealing condition is found to be very important for improving short circuit current, fill factor and therefore the efficiency of the device [14].

Thermal annealing can be done either before cathode deposition or after cathode deposition. It is reported that, thermal annealing before cathode deposition induces change in crystal structure of active layer, while thermal annealing after cathode deposition induces the variation in crystal structure and variation in the contact between active layer and cathode as well. In this study, we report recent advances directed towards the optimization of organic polymer-fullerene BHJ solar cells, also employing ZnO nanoparticles as electron transporting layer in the context of how they have redefined the fundamental understanding of energy conversion to improve performance [14]. We also discuss the inverted geometry of organic solar cells to compare the performance to the normal/conventional geometry.

## EXPERIMENTAL

*(A) ZnO nanoparticles synthesis*

ZnO nanoparticles were synthesized by hydroxylation of zinc acetate dihydrate ($ZnAc.2H_2O$) by tetramethylammonium hydroxide (TMAH). In a typical preparation, TMAH dissolved in 30 ml of ethanol was added dropwise to 0.1M zinc acetate dihydrate dissolved in 30 ml of dimethylsulfoxide (DMSO) followed by vigorous stirring for 1hour at room temperature. Nanoparticles were precipitated by adding ethyl acetate. The precipitate was separated by centrifugation and was washed at least three times by a mixture of heptane and ethyl acetate in the volume ratio of 2:1 and then in heptane only. The ZnO nanoparticles were either dispersed in methanol or dried in an oven kept at 110$^o$C for 1hour.

*(B) ZnO nanoflake and nanoflower synthesis*

ZnO nanoflakes were synthesized by adding a mixture of polyethyleneglycol (PEG) ($M_w$=1000) and ammonia water ($NH_3.H_2O$) dropwise to 0.2M solution of zinc nitrate hexahydrate ($Zn(NO_3)_2.6H_2O$) resulting in a white mixture with pH of 12. The mixture was rapidly stirred at 60$^o$C for 1 hour. The precipitate was centrifuged and washed at least three times with ethanol and distilled water and was then dried in an oven at 110$^o$C for 1hour. Similar experimental procedure was followed to prepare ZnO nanoflowers structures except that the mixture was vigorously stirred for 10 hours.

*(C) Device fabrication*

*(i) Conventional geometry*

The device geometry was ITO/PEDOT:PSS/P3HT:PCBM/ZnO nanopaticles/Al with the device area of 0.12 $cm^2$. A glass substrate pre-coated with ITO and modified by spin-coating a thin layer of PEDOT:PSS followed by drying in an oven/hot plate at 110 $^o$C for 10 min was used as an anode electrode. The photoactive layer of P3HT:PCBM blend with a weight ratio of 1:0.6, dissolved in chlorobenzene, was spin-coated at the speed of 1000 rpm for 15 s. This was followed by the deposition of the layer of methanol solution of ZnO nanoparticles at 4000 rpm for 35 s. Finally, the top Al metal electrode (100 nm) was thermally evaporated at ~ 1 x $10^{-6}$ Torr pressure through a shadow mask defining the device area. Pre and post-annealed devices are compared in this study, i.e. Devices that was then thermally treated before the evaporation of Al electrode (i.e. pre-annealing) and devices that was thermally treated after the evaporation Al electrode (i.e. post-annealing) at 155 $^o$C for 10 min. we also compare the devices with ZnO nanoparticles and nanoflakes ETL.

*(ii) Inverted geometry*

The inverted devices with the device area of 0.12 $cm^2$ were fabricated. The ZnO (spherical particles and nanoflowers) layer from methanol solution was spin-coated at 4000 rpm for 35 sec on top of ITO/glass substrate and was dried on a hot plate at 60-$^o$C for 1 hour. The photoactive layer of P3HT:PCBM blend with a weight ratio of 1:0.6, dissolved in chlorobenzene, was spin-coated with the speed of 1000 rpm for 15 sec followed by PEDOT:PSS layer. The next step was to evaporate the ~ 100 nm silver (Ag) metal electrode at ~ 1× $10^{-6}$ Torr and the cells were annealed at 155 $^o$C for 10 min.

*(D) Characterization*

The structure of nanoparticulate ZnO and particle morphology were studied using X-ray diffraction (XRD, Bruker AXS D8 Advanced) and field-emission scanning electron microscopy (FE-SEM, Nova-nano SEM200), respectively. The current density-voltage (J-V) curves were measured in air using a Keithley 2400 source meter and an Oriel xenon lamp (150 W) coupled with an AM1.5 filter to simulate sunlight. The light intensity was calibrated with a silicon reference cell with a KG2 filter following standard solar cell testing procedures. All J-V measurements were conducted at the light intensity of 100 $mW/cm^2$. The external quantum efficiencies (EQE) as a function of wavelength were measured using an incident photon-to-current efficiency (IPCE) measurement system (PV measurement, Inc). The wavelength of the bias light was controlled with optical filters (Andover Corporation).

## RESULTS AND DISCUSSION

Figure 1(a-b) shows the conventional and the inverted geometry of devices. The organic solar cells comprises of an active layer sandwiched between a transparent conductive oxide (ITO) coated glass as an anode and/or cathode electrode and a top metal electrode Al and/or Ag. PEDOT:PSS is the hole transporting layer in both geometries. Although PEDOT:PSS is usually used to modify the transparent ITO in conventional structure for efficient collection of holes, due to its strong acidic nature the degradation of ITO/PEDOT:PSS is inevitable [15], therefore the polarity of ITO is reversed by inserting the ZnO electron extracting layer and using the high work function metal Ag in inverted geometry. In this type of a structure, the elimination of PEDOT:PSS and prevention of air and moisture diffusion by using Ag metal electrode can also improve the stability of the device [16]. Incorporation of a solution processed ZnO nanoparticles serves as an electron transporting layer and at the same time can block holes from reaching the top Al metal electrode. Furthermore it acts as the buffer layer preventing the Al atoms from diffusing into the active layer [17]. Both kinds of devices comprise of a similar cathode structure formed by ZnO layers, with the main difference being the deposition order.

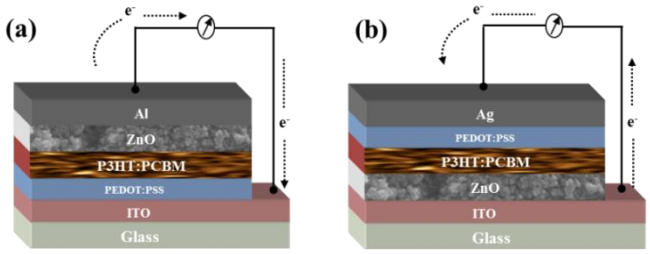


Figure 1: (a) conventional and (b) inverted organic solar cells

Figure 2 shows the XRD pattern of spherical nanoparticles, nanoflakes and nanoflowers. The patterns exhibited the hexagonal wurtzite structure of ZnO matching the standard JCPDS data, card no 80-0075. The average crystallite size of nanoparticles was estimated using the Debye-Scherrer equation [18] and was found to be ~ 5 ± 0.2 nm in diameter, ~20 ±0.2 nm and ~35 ± 0.2 nm for nanoparticles, nanoflakes and nanoflowers, respectively. Figure 3(a-b) shows FE-SEM images of spherical nanoparticles and randomly oriented nanoflakes. Flower-like clusters were also observed (fig 3(c)), they have symmetric arms in level directions. Every arm consists of cluster of nanoparticles. Figure 3(d-f) also shows the cross-sectional view of conventional device and the device image showing four cell areas (fig 3d). Device layers are clearly identified and fine layer of ZnO nanoparticles is uniformly distributed and cluster of nanoflakes, whereas the nanoflowers were just scattered on the surface (note that fig 3f shows distribution of nanoflakes from just an glass/ITO substrate). We used the ZnO nanoparticles as ETL and for light scattering to increase light absorption without having to increase the electron donor (P3HT) thickness. If the straight incident photons hit nanoparticles, the photons would be refracted and many part of the incident photons would move to the side. This may cause a lot of photons to be absorbed therefore excitons can be created nearby acceptor (PCBM) material.

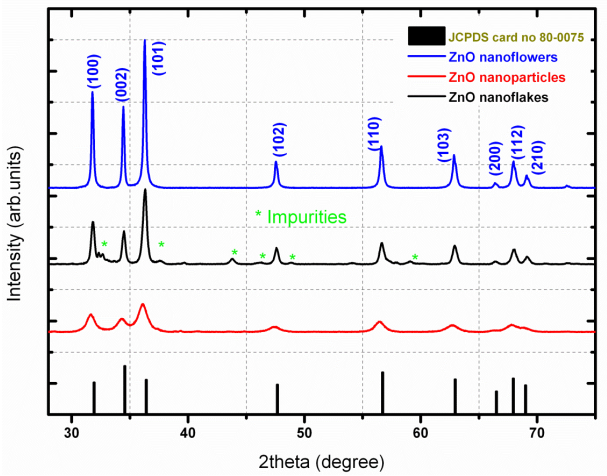


Figure 2: XRD patterns of ZnO nanostructures and standard JCPDS data.

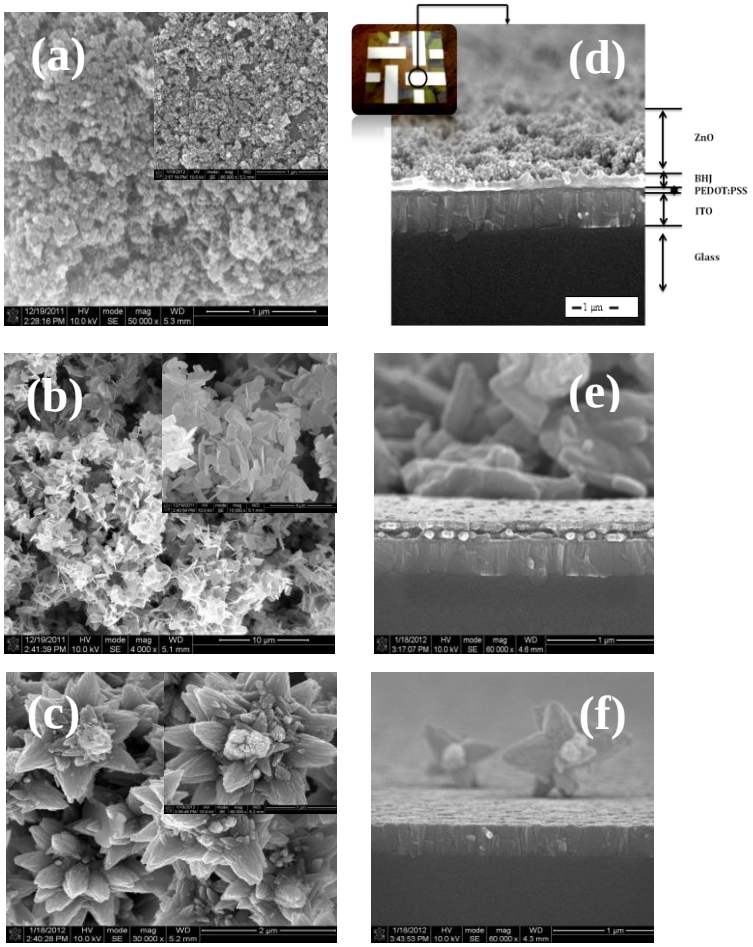


Figure 3: FE-SEM images of (a) ZnO spherical-particles, (b) nanoflakes, (c) nanoflowers and (d-f) cross-sectional view.

The photovoltaic response of devices with ZnO nanoflakes electron transporting layers spin-coated from solutions of different concentration of ZnO is illustrated by the J-V curves shown in figure 4(a) and (c) and the summary of the PV characteristics is presented in table 1. The current-voltage characteristics show that the device performance is greatly improved by the thermal treatment after the deposition of an Al electrode. The PCE is significantly increased from 0.31 % to 3.08 %, with the highest efficiency being observed from the device with 0.5 mg/mL ZnO concentration. Similarly, the same trend was observed with the device having 0.5 mg/mL ZnO concentration (spherical nanoparticles). The efficiency improved from 0.17 % to 2.37 %. The J-V curves for these devices are shown in figure 5(a) and PV summary is shown on table 2 .However, there was no efficiency recorded for the pre-annealed devices for this batch of experiment (i.e. Devices with ZnO nanoparticles). In addition the $V_{oc}$ of post-annealed devices marginally improved from high concentration of ZnO to the lowest, in both cases of nanoparticles and nanoflakes. One possible reason might be the increased contact area between the ETL and metal cathode which result in a more efficient charge collection at the interface [20]. Diffusion length of charge carriers in organic materials is often only few nanometers and only those carriers generated near the electrodes will be collected and give rise to a photo-current [20]. Therefore the increased contact area will most probably have an effect on the efficiency of charge collection [20]. We can also attribute the improved efficiency of post annealed devices to the combined effects of ETL and annealing treatment. The external quantum efficiency (EQE) curves are shown in figure 4(b and d) and figure 5(b). For devices with ZnO nanoflakes ETL, the maximum photocurrent contribution is observed to be almost 20% more in post-annealed devices compared to the pre-annealed devices with the device having 0.5 mg/mL ZnO concentration.

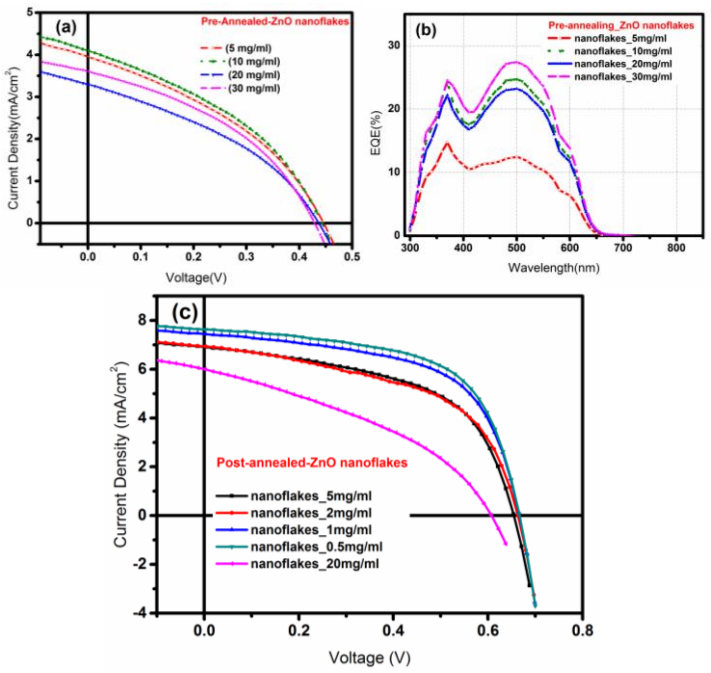


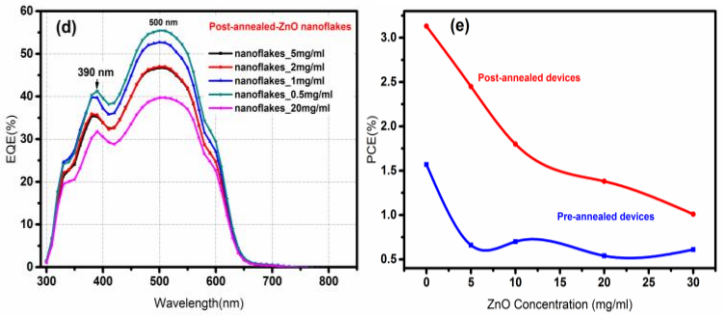


Figure 4: (a-c) J-V curves ,(b-d) EQE curves of OSC devices annealed before and after depositing the top Al electrode and (e) PCE vs ZnO nanoflakes concentration

**Table 1:** Photovoltaic properties of post-annealed devices with ZnO nanoflakes buffer layer

| P3HT:PCBM Weight ratio | ZnO conc(mg/ml) | $J_{sc}$(mA/cm$^2$) | $V_{oc}$(V) | FF(%) | PCE(%) |
|---|---|---|---|---|---|
| 1:0.6 | Nanoflakes ~ 0.5 | 7.632 | 0.666 | 60.61 | 3.08 |
| 1:0.6 | Nanoflakes ~ 1 | 7.446 | 0.666 | 59.18 | 2.94 |
| 1:0.6 | Nanoflakes ~ 2 | 6.939 | 0.663 | 52.81 | 2.43 |
| 1:0.6 | Nanoflakes ~ 5 | 6.915 | 0.654 | 54.18 | 2.45 |
| 1:0.6 | Nanoflakes ~ 10 | 6.353 | 0.634 | 44.72 | 1.80 |
| 1:0.6 | Nanoflakes ~ 20 | 6.006 | 0.607 | 37.78 | 1.38 |
| 1:0.6 | Nanoflakes ~ 30 | 5.944 | 0.494 | 34.37 | 1.01 |
| 1:0.6 | Nanoflakes ~ 40 | 9.591 | 0.482 | 33.03 | 0.89 |
| 1:0.6 | Nanoflakes ~ 50 | 3.386 | 0.304 | 30.46 | 0.31 |

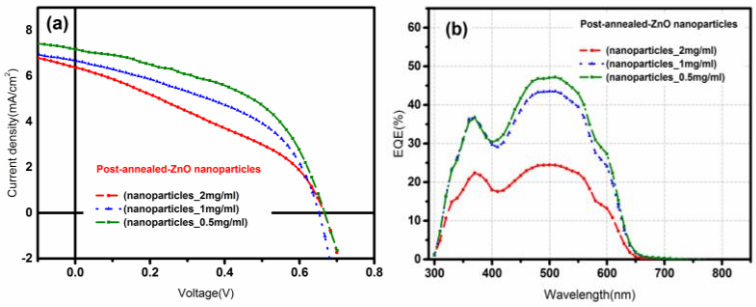


Figure 5: (a) J-V curves and (b) EQE curves of OSC devices annealed after depositing the top Al electrode

**Table 2:** Photovoltaic properties of post-annealed devices with ZnO nanoparticles buffer layer

| P3HT:PCBM Weight ratio | ZnO coc(mg/ml) | $J_{sc}$(mA/cm$^2$) | $V_{oc}$(V) | FF(%) | PCE(%) |
|---|---|---|---|---|---|
| 1:0.6 | Nanoparticles ~ 0.5 | 7.179 | 0.667 | 49.55 | 2.37 |
| 1:0.6 | Nanoparticles ~ 1 | 6.672 | 0.652 | 45.57 | 1.96 |
| 1:0.6 | Nanoparticles ~ 2 | 6.383 | 0.666 | 35.70 | 1.52 |
| 1:0.6 | Nanoparticles ~ 5 | …… | …… | …… | …… |
| 1:0.6 | Nanoparticles ~ 10 | …… | …… | …… | …… |
| 1:0.6 | Nanoparticles ~ 20 | 0.744 | 0.641 | 36.28 | 0.17 |
| 1:0.6 | Nanoparticles ~ 30 | …… | …… | …… | …… |

The influence of ZnO particle morphology was investigated. Figure 6(a) compares the J-V curves of devices with ZnO nanoparticles and nanoflakes layers spin-coated from solutions of 0.5 mg/mL concentration. The PV performance parameters are summarized in tables 1 and 2. The higher PCE efficiency of 3.08 % was recorded from ZnO nanoflakes device and 2.37 % was recorded from device with ZnO nanoparticles. This suggests that ZnO nanoflakes ETL made relatively superior contact with the photo-active layer and the top metal electrode compared to the nanoparticles. Liang et al [21] have pointed out that the surface quality of the ZnO layer can lead to improved photovoltaic properties of the devices. In addition, rougher interface between photo-active layer and the top metal electrode can improve the efficiency by increasing light scattering thereby enabling increased light harvest in the photo-active layer and subsequently preventing the formation of shunt paths [5,23]. As discussed it is reasonable to attribute the high PCE value of 3.08 % from the device with ZnO nanoflakes to increased light harvest by rougher interfacial morphology. The improvement in device performance is observed from the EQE of the devices, as shown in figure 6(b). There is a significant increase in EQE for the device with ZnO nanoflakes ETL with maximum of ~55% at the wavelength of ~505 nm versus ~47% for the ZnO nanoparticles ETL. Several factors contribute to the functionality of the devices at the interfaces. By evaluating the series resistance ($R_s$) and shunt resistance ($R_{sh}$) in a device, we can determine the impact of the contacts between the buffer layer and the photo-active layer, the buffer layer and the top electrode on the general performance of the devices. Good contact between the ZnO layer and the photoactive layer can decrease $R_s$ by improving collection and transportation of electrons to the cathode and poor contact between the ZnO layer and the photoactive layer and between the ZnO layer and the top electrode can lead to low shunt resistance values and a subsequent low PCE due to creation of alternative current paths. Table 3 presents $R_s$ and $R_{sh}$ values independently calculated from the inverse slope of the J-V curves of the devices at I = $J_{sc}$ (V = 0) and V = $V_{oc}$ (I = 0), respectively. The Rs values increases with an increase of the ZnO concentration, resulting in the decrease of PCE while the $R_{sh}$ increases with a decrease of the ZnO concentration resulting in the increase of the FF, $J_{sc}$ and PCE values. This data is consistent with the data reported by Liang et al [21] and suggests that due to superior contact, ZnO nanoflakes serve as better transport pathways for electrons and the parasitic losses are lower than those of ZnO nanoparticles.

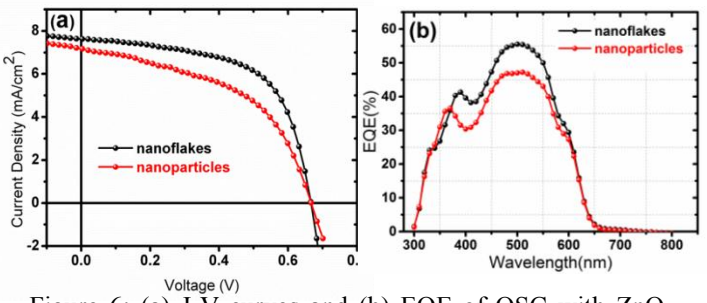


Figure 6: (a) J-V curves and (b) EQE of OSC with ZnO nanoparticles and nanoflakes devices annealed after depositing the top Al electrode.

**Table 3:** Series and Shunt Resistance comparison of P3HT:PCBM solar cells with different concentrations of ZnO nanoparticles and nanoflakes

| Concentration (mg/ml) | ZnO nanoparticles | | ZnO nanoflakes | |
|---|---|---|---|---|
| | $R_s$ ($\Omega$.cm$^2$) | $R_{sh}$ ( $\Omega$.cm$^2$) | $R_s$ ($\Omega$.cm$^2$) | $R_{sh}$($\Omega$.cm$^2$) |
| 0.5 | 217 | 2900 | 114 | 6300 |
| 1 | 318 | 2650 | 129 | 5890 |
| 2 | 295 | 1850 | 294 | 4260 |
| 20 | 2500 | 9690 | 377 | 1940 |

Figure 7(a) compares the current density-voltage (J-V) characteristics of an inverted device with ZnO nanoparticle and nanoflowers. The extracted device parameters are summarized in Table 4. Overall, we notice that the photovoltaic response of the device with ZnO nanoparticles shows a $J_{sc}$ of 8.33mA/cm$^2$, $V_{oc}$ of 0.58 V and FF of 46.45 %, resulting in the PCE of 2.26-%. However, as shown in table 4, the PV values from the device with ZnO nanoflowers were comparatively low with the PCE of 1.08%. It is evident from the J-V curve that the device with nanoflowers suffers the high series resistance. Since these devices are fabricated with the same materials and the same procedure and the only difference is the electron extraction layer morphology, the increased current density is unlikely to account for other reasons, but possibly due to reduced series resistance in the case of ZnO nanoparticles. Shim et al [4], have demonstrated that the tuning of ZnO buffer layer in inverted devices improves the photovoltaic performance and the stability of the device. However, when the ZnO buffer layer becomes thick, a high intrinsic resistance increasing the series resistance and reducing the charge carrier transport ability can decrease the photovoltaic performance of the device [4]. The external quantum efficiencies (EQE) of these two devices are compared in figure 7(b). The device with the ZnO nanoparticles clearly has a higher EQE, especially for wavelengths longer than ~ 450 nm. The EQE of the device with ZnO nanoparticles exceeds that of the nanoflowers by approximately 10%. A slight red-shift of spectrum is also observed. The enhanced or red-shift is attributed to be the result of improved polymer chain ordering from the growth process due to heat treatment [22].

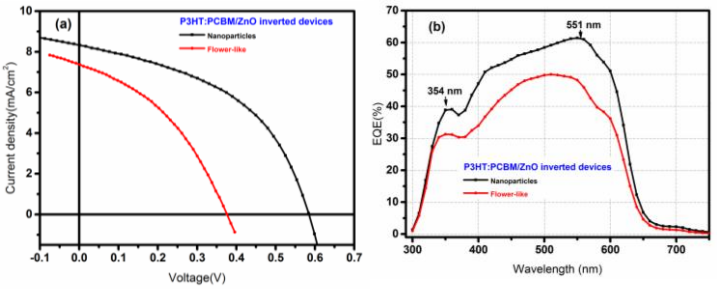


Figure 7: (a) J-V curves and (b) EQE curves of OSC devices for inverted geometry with nanoparticles and nanoflowers

**Table 4:** Photovoltaic properties of inverted geometry devices

| Inverted Device | ZnO Layer | $J_{sc}$ (mA/cm$^2$) | $V_{oc}$ (V) | FF(%) | PCE(%) |
|---|---|---|---|---|---|
| (1) | Nanoparticles | 8.331 | 0.5848 | 46.45 | 2.26 |
| (2) | Flower-like | 7.379 | 0.3763 | 38.81 | 1.08 |

## CONCLUSION

We have reported the use of ZnO nanoparticles buffer layer and/or electron transporting layer (ETL) for a better understanding of how to improve the PV properties of organic solar cells. An improvement in PV properties was observed from the post annealed devices compared to a similar device but annealed before the deposition of top electrode (pre-annealed). Devices with ZnO nanoflakes and nanoparticles electron extraction layers spincoated from solutions of 0.5 mg/mL concentration with the nanoflakes showed a relatively high PCE value of 3.08% versus 2.37% from the nanoparticles. We also observed that the PV properties of conventional devices depended on the concentration and morphology of ZnO ETL. PV parameters of inverted geometries were compared and found that the morphology of ZnO had an impact on the performance of organic solar cells and the higher PCE of 2.26 % was obtained from the device with ZnO nanoparticles layer.

## REFERENCES


[1] D. Olson, Y.-J. Lee, M.S. White, N. Kopidakis, S.E. Shaheen, D.S. Ginley, J.A. Voigt and J.W.P. Hsu, Effect of polymer processing on the performance of poly(3-hexylthiophene)/ZnO nanorod photovoltaic devices, *Journal of Physical Chemistry B*, vol.111, 2007, pp.16640-16645

[2] H. Oh. J. Krantz, I. Litzov, T. Stubhan, L. Pinna and C.J. Brabec,Comparison of various sol-gel derived metal oxide layers for inverted organic solar cells, *Solar Energy Materials and Solar Cells*, vol.95, 2011, pp. 2194-2199

[3] L. Quian, J. Yang, R. Zhou, A. Tang, Y. Zheng. T.-K. Tseng, D. Bera, J. Xue and P.H. Holloway, Hybrid polymer-CdSe solar cells with ZnO nanoparticle buffer layer for improved efficiency and lifetime, *Journal of Materials Chemistry*, vol.21, 2011, pp. 3114-3817

[4] W.H. Shim, M.Y. Park, D.S. Park, Y.T. Kim, S.Y. Park, J.-H. Lim, K.H. Lee. Y.S. Jeong, Y.D. Kim, K.-D. Kim, H.O. Seo, Y.D. Kim and D.C. Lim, Effects of sol-gel prepared ZnO electron selective layer on the performance of inverted organic solar cells, *Molecular Crystal and Liquid Crystal*, vol.538, 2011, pp. 164-170

[5] O.M. Ntwaeaborwa, R. Zhou, L. Qian, S.S. Pitale, J. Xue, H.C. Swart and P.H. Holloway, Post-fabrication annealing effects on the performance of P3HT:PCBM solar cells with/without ZnO nanoparticles, *Physica B*, vol.407, 2012, pp. 1631-1633

[6] K.-F. Lin, H.-M. Cheng, H.-C. Hsu, L.-J. Lin and W.-F. Hsieh, Band gap variation of size-controlled ZnO quantum dots synthesized by sol-gel method, *Chemical Physics Letters*, vol.409, 2005, pp. 208-211

[7] H. Zhang, J. Feng, J.Wang and M. Zhang, Preparation of ZnO nanorods through wet chemical method, *Materials Letters*, vol.61, 2007, pp. 5202-5205

[8] X. Hou, L. Wang, B. Yu, F.Zhoo and W.Liu, Synthesis of branched ZnO nanorods on various substrates via a wet chemistry route, *Particuology*, vol.8, 2010, pp.458-462

[9] Y.W Chen, Q. Qias, Y.C Liu, and G.L Yang, *Journal of Physical Chemistry*, vol.113, 2009, pp.7494-7502

[10] Y. J. Kwon, K. H. Kim, C. S. Lim and K. B. Shim, Characterization of ZnO Nanopowders Synthesized by the Polymerized Complex Method via an Or-ganochemical Route, *Journal of Ceramic Processing Research*, Vol. 3, No. 3, 2002, pp. 146-149.

[11] Y. Lare, A.Codoy, L. Cattin, K. Jondo, T. Abachi, F.R. Diaz, M. Morsli, K. Napo, M.A. del Valle and J.C Bernede, ZnO thin films fabricated by chemical bath deposition used as a buffer layer in organic solar cells, *Applied Surface Science*, vol.255, 2009, pp. 6615-6619

[12] C. Wu, X. Qiao, J. Chen, H. Wang, F.Tan and S.Li, A novel chemical route to prepare ZnO nanoparticles, *Materials Letters*,vol.60, 2006, pp.1828-1832

[13] L.Chang, H.W.A Lademann, J-B Bonekamp, K.Meerholz and A..J Moule, Effects of trace solvent on the morphology of P3HT:PCBM bulk heterojunction solar cells, *Advanced Functional Materials*, vol.21, 2011, pp.1779-1787

[14] G. Li, V. Shrotriya, Y. Yao and Y. Yang, Investigation of annealing effects and film thickness dependence of polymer solar cells based on poly(3-hexylthiophene), *Journal of Applied Physics*, vol.98, 2005, pp.043704-1 -043704-5

[15] K.W. Wong, H.L. Yip, Y. Luo, K.Y. Wong, W.M. Lau, K.H. Low, H.F. Chow, Z.Q. Gao, W.L. Yeung and C.C Chang, Blocking reactions between indium-tin oxide and poly(3,4-ethylene dioxythiophene):poly(styrene sulphonate) with a self-assembly monolayer, *Applied Physics Letters*, vol.80, 2002, pp.2788-2790

[16] F.C Krebs, S.A. Gevorgyan and J. Alstrup, A roll-to-roll process to flexible polymer solar cells, *Journal of Materials Chemistry*, vol.19, 2009, pp.5442-5451

[17] K. Lee, J.Y. Kim, S.H. Park, S.H. Kim, S. Cho and A.J. Heeger, Air stable polymer electronic devices, *Advanced Materials*, vol.19, 2007, pp.2445-2449

[18] S. Tachikawa, A. Nogushi, T. Tsuge, M. Hara, O. Odawara and H. Wada, Optical properties of ZnO nanoparticles capped with polymers, *Materials*, vol.4 ,2011, pp.1132-1143

[19] K.Kim, B. Jung, J. Kim and W.Kim, *Proceedings of PowerMEMS workshop*, 2009, pp.1-4

[20] P. Peumans and S. R. Forrest, Very-High-Efficiency Double-Hetero-Structure Copper Pthalocyanine/C60 Photovoltaic Cells, *Applied Physics Letters*, Vol. 79, No. 1, 2001, pp.126-128

[21] Z. Liang, Q. Zhang, O. Wiranwetchayan, J. Xi, Z. Yang, K. Park, C. Li and G. Cao, Effects of morphology of a ZnO buffer layer on the photovoltaic performance of inverted polymer solar cells, *Advanced Functional Materials* vol.22, 2012 ,pp.2194-2201

[22] V. Shrotriya, G. Li, Y.Yao, T. Moriarty, K. Emery and Y. Yang, Accurate measurements and characterization of organic solar cells, *Advanced Functional Materials*, vol.16, 2006, pp.2016-2023